Applied and Computational Mechanics 18 (2024) 175–188

Effect of spin slip conditions on Couette-Poiseuille flow of couple stress fluid between parallel plates

S. Nishad[a], K. P. Madasu[a,*]

[a] Department of Mathematics, National Institute of Technology Raipur, 492010, Chhattisgarh, India

Received 8 July 2024; accepted 10 December 2024

Abstract

In the current paper, we investigate the effect of spin slip conditions for the Couette-Poiseuille flow of a couple stress fluid between two parallel plates. In the study, the motion of the fluid is considered to be steady, incompressible and unidirectional. At the interface between the fluid and the plates (both the upper and lower), we consider the non-zero tangential and couple stress spin slip relationships as boundary conditions. We present analytical expressions for the velocity profile, volume flow rate, vorticity, and couple stresses. This paper discusses the numerical influence of the spin slip parameter, velocity slip parameter, couple stress parameter, and pressure gradient on the velocity, vorticity, couple stresses, and volume flow rate. Our results show that the presence of the spin slip parameter reduces the velocity, couple stress and volume flow rate of the fluid, while it enhances the vorticity. The limiting cases for each problem align well with previously published results regarding the vanishing of couple stresses at the boundaries. This research helps both researchers and engineers in understanding how to control the conditions to achieve an efficient fluid flow, particularly in applications involving couple stress effects, such as microfluidics systems, lubrication technology, and polymeric suspensions.

Keywords: Couette flow, Poiseuille flow, generalized Couette flow, couple stress fluid, exact solutions, spin slip effect

1. Introduction

A fluid that opposes the Newton's law of viscosity is commonly referred to as a non-Newtonian fluid and has a wide range of usage in the industrial and technological sectors. Custard, shampoo, blood, paint, starch, cornstarch, ketchup and other substances are non-Newtonian fluids. One specific type of non-Newtonian fluids is called a couple stress fluid, which illustrates the influences of body couples and couple stresses in a fluid medium. This theory was proposed by Vijay Kumar Stokes in the 20$^{\text{th}}$ century. Over the past 50 years, it has captured the interest of several fluid mechanics researchers. According to this theory, the stress tensor is antisymmetric and the rotation vector is defined as half of the curl of the velocity vector. There are numerous scientific and industrial applications for this concept. Modelling the flows of manufactured fluid, animal blood, liquid crystals, lubrication, and polymer-thickened oils can be done using the couple stress theory [9, 21].

Many researchers have applied the tangential slip conditions to investigate the various fluid flow problems. In [5], Ashmawy examined the unsteady problem of a micropolar fluid flow confined between two parallel plates by implementing slip boundary conditions at the lower and upper plates. He observed that the velocity, microrotation, and total flux increase with higher slip parameters. Using the homotopy analysis method, Ellahi [12] studied the impact of slip

*Corresponding author. Tel.: +91 957 550 84 47, e-mail: madaspra.maths@nitrr.ac.in.
https://doi.org/10.24132/acm.2024.912

conditions on the fundamental flows of an Oldroyd 8-constant fluid. In [17], Navier provided a velocity slip boundary condition that establishes a proportional relationship between the shear rate and the tangential velocity at the solid surface of the fluid. In recent years, significant interest has arisen in determining approximate boundary conditions for fluid flow in complex geometries, largely due to advancements in microelectromechanical systems. Neto et al. [18] proposed an experimental study of Newtonian fluid slip at solid surfaces, which enhances our understanding of hydrodynamic boundary conditions that can be used to actively control fluid slip.

The study of classical flow problems is crucial in understanding biophysical and technological flows. Examples of fluid flow applications can be found in the cosmetic industry, transpiration cooling, and inkjet printers. The classical flows serve as benchmarks to compare outcomes from flow problems with complex geometries and to provide precise solutions to the governing equations. Numerous researchers have analyzed the fundamental fluid flow problems in light of broader applications. For instance, Ramesh [19] derived analytical solutions for the classical problem of incompressible Jeffrey flow using parallel plate geometry, by considering the effects of magnetohydrodynamic (MHD) and radiation. In [13], Hayat et al. found both numerical and analytical solutions for the Couette and Poiseuille flows of an Oldroyd 6-constant fluid under electric and MHD effects. Chain and Zhu [8] examined the Couette and Poiseuille flow problems of Bingham fluids between porous plates, utilizing the Beavers and Joseph's model. Devakar et al. [10] derived analytical solutions for various classical flows of an incompressible couple stress fluid. Zeeshan et al. [22] addressed the flow of nanofluids through porous wavy channels, considering the effects of temperature and magnetic and electric fields. Alamri et al. [3] studied the impact of velocity slip on the nanofluid flow between two parallel plates under Stefan blowing and MHD effects. Additionally, many interesting problems related to the unsteady flow of micropolar and couple stress fluids can be found in [1, 2, 6, 7, 15].

This paper examines the impact of spin slip conditions for three fundamental flows. The conditions allow for the consideration of slip in rotational motion, which is helpful for understanding flow near porous or rough surfaces, as well as in microscale flows, where boundary interactions can be complex. To the best of authors' knowledge, this study has not been conducted before. The tangential and spin slip conditions are applied at both plates. Here, three cases are analyzed:

1. In the first case, both stationary plates move with various translatory constant velocities while the fluid particles rotate. Additionally, the pressure gradient is zero in this case.
2. In the second case, fluid flow occurs due to a pressure gradient, with fluid particles rotating around their positions.
3. The third case considers a pressure gradient that induces flow, with the upper plate translating at a constant velocity. However, the lower plate remains stationary and all fluid particles are rotating.

This research extends the work of Devakar et al. [10] by applying the spin slip conditions in couple stress fluid flows between two parallel plates. These classical flow problems are fundamental to various applications, including microfluidics, industrial processes, and fluid flow in pipes, such as fuel dispersion in engines. In all these applications, viscosity, pressure and slip parameters directly affect the velocity and volume flow rate, influencing the overall efficiency of the fluid flow process.

2. Mathematical model and solution

The governing equations for an incompressible and steady couple stress fluid flow in the absence of body couple and body forces are given as [21]

$$\nabla \cdot \boldsymbol{v} = 0, \tag{1}$$

$$\nabla p + \mu \nabla^2 \boldsymbol{v} + \eta \nabla^4 \boldsymbol{v} = 0, \tag{2}$$

where $\boldsymbol{v}$, p, μ, and η denote the velocity, the pressure, the classical fluid viscosity coefficient and the first couple stress viscosity coefficient, respectively. The stress tensor t_{ij} and the couple stress tensor m_{ij} of the fluid are given as [16, 21]

$$t_{ij} = -p\,\delta_{ij} + 2\mu d_{ij} - \frac{1}{2}\varepsilon_{ijk} m_{sk,s}\,, \qquad m_{ij} = m\delta_{ij} + 4\,\eta\,\omega_{i,j} + 4\,\eta'\,\omega_{j,i}\,, \tag{3}$$

where m, $\omega_{i,j}$, $d_{i,j}$, ε_{ijk}, δ_{ij}, and η' denote the trace of the couple stress tensor, the spin tensor, the deformation rate tensor, the alternating tensor, the Kronecker delta and the second viscosity coefficient of a couple stress fluid, respectively. The material constants satisfy the following inequalities [16, 21]:

$$\mu \geq 0, \quad \eta \geq 0, \quad \eta \geq \eta' \geq -\eta.$$

The Kronecker delta δ_{ij}, the deformation rate tensor d_{ij}, and the alternating tensor ε_{ijk} are defined as [16, 21]

$$\delta_{ij} = \begin{cases} 0 & \text{for } i \neq j, \\ 1 & \text{for } i = j, \end{cases} \qquad d_{ij} = \frac{1}{2}(v_{i,j} + v_{j,i}), \qquad \varepsilon_{ijm} = \begin{cases} 1 & \text{for } \varepsilon_{123}, \varepsilon_{231}, \varepsilon_{312}, \\ -1 & \text{for } \varepsilon_{132}, \varepsilon_{321}, \varepsilon_{213}, \\ 0 & \text{otherwise.} \end{cases}$$

The vorticity vector ω is defined as [21]

$$\omega = \frac{1}{2}\varepsilon_{ijk} v_{k,j}. \tag{4}$$

For the problem under the consideration of unidirectional steady flow, we assume a velocity field in the following form:

$$\boldsymbol{v} = (u(y), 0, 0). \tag{5}$$

Then, equation (2) reduces to

$$\eta \frac{d^4 u}{dy^4} - \mu \frac{d^2 u}{dy^2} + \frac{dp}{dx} = 0. \tag{6}$$

To obtain (6) in dimensionless form, we used the following non-dimensional variables [10, 14]:

$$\tilde{y} = \frac{y}{l}, \quad \tilde{x} = \frac{x}{l}, \quad \tilde{u} = \frac{u}{u_1}, \quad s^2 = \frac{\eta}{\mu l^2}, \quad \tilde{p} = \frac{p\,l}{\mu\,u_1}.$$

After dropping the symbol (˜), equation (6) becomes

$$s^2 \frac{d^4 u}{dy^4} - \frac{d^2 u}{dy^2} = G, \tag{7}$$

where $s = \sqrt{\eta / (\mu l^2)}$ is the couple stress parameter and $G = -\frac{dp}{dx}$ is the pressure gradient. If $s \to 0$, the case of a classical fluid is obtained.

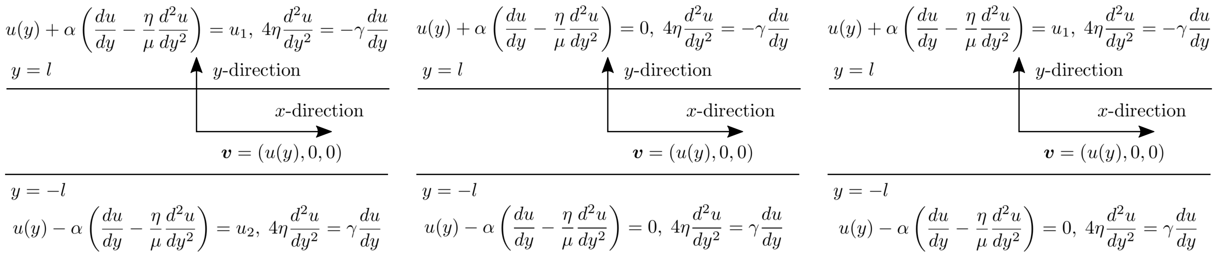

(a) Couette flow (b) Poiseuille flow (c) generalized Couette flow

Fig. 1. Three types of flow between two parallel plates

The general solution of the fourth order differential equation (7) is given as

$$u = A_i + B_i\, y + C_i\, e^{y/s} + D_i\, e^{-y/s} - \frac{Gy^2}{2}. \tag{8}$$

The formulas for the shear stress, the vorticity, the couple stress and the volume flow rate are [10, 21]:

$$t_{yx} = \frac{du}{dy} - s^2\frac{d^3u}{dy^3}, \qquad \omega_z = -\frac{1}{2}\frac{du}{dy}, \qquad m_{yz} = 4\eta\frac{d\omega_z}{dy}, \qquad Q = \int_{-l}^{l} u\, \mathrm{d}y.$$

2.1. Boundary conditions

To find the solution of the above described problem, we need four boundary conditions to obtain the arbitrary constants A_i, B_i, C_i, and D_i for the plane Couette flow ($i = 1$), the plane Poiseuille flow ($i = 2$), and the generalized Couette flow ($i = 3$), Fig. 1. In this analysis, we applied two hypotheses: (i) tangential slip boundary conditions and (ii) mixed type boundary conditions, which were firstly assumed by Navier [17] and Stokes [21], respectively. The inclusion of spin slip conditions enhances the realism and practicality of the flow model and should be used with tangential slip conditions. The concept of spin slip is often utilized in studying fluid flow models that involve microstructures, such as polymers, biological fluids, and liquid crystals. In these cases, the internal rotations and couple stress effects are crucial for analysis. Since the couple stress fluids allow for the consideration of both shear stress and rotational effects, the slip influences the effective viscosity and boundary layer properties in the fluid flow models, where the influence of couple stress effects is significant. The slip arises from the characteristics of both the surface and the fluid. The spin slip conditions along with tangential slip conditions are used to solve the problem for the present investigation. Recently, several researchers [4, 11, 21] have implemented spin slip conditions on solid surfaces.

(i) *The tangential slip boundary conditions* – the relative velocity between the plates and the fluid is proportional to the shear stress at the plates [10]:

$$u(-l) - u_2 = \alpha\left(\frac{du}{dy} - \frac{\eta}{\mu}\frac{d^3u}{dy^3}\right)\bigg|_{y=-l}, \qquad u(l) - u_1 = -\alpha\left(\frac{du}{dy} - \frac{\eta}{\mu}\frac{d^3u}{dy^3}\right)\bigg|_{y=l}. \tag{9}$$

(ii) *The couple stress spin slip conditions* – vorticity at the boundary is directly proportional to the rate of rotation of the boundary [4, 11, 21]:

$$4\,\eta\frac{d^2u}{dy^2}\bigg|_{y=-l} = \gamma\frac{du}{dy}\bigg|_{y=-l}, \qquad 4\,\eta\frac{d^2u}{dy^2}\bigg|_{y=l} = -\gamma\frac{du}{dy}\bigg|_{y=l}, \tag{10}$$

where α and γ are the velocity and couple stress spin slip parameters, respectively. The parameters depend on nature of plate surface and fluid. In both engineering and biological contexts, the slip parameters are crucial for accurately predicting flow behavior near interfaces. This accuracy is essential for designing systems that involve microstructured fluids. For $\alpha \to 0$, equations (9) denote the no slip conditions and if $\alpha \to \infty$, they represent perfect slip conditions. Also, for $\gamma \to 0$, equations (10) indicate the vanishing couple stress at the boundaries, it indicates the mechanical interactions of fluid particles at the plates surface are equivalent to a force distribution, while $\gamma \to \infty$, there is no relative rotation of fluid particles.

2.2. Plane Couette flow (CF)

Let us consider steady flow of an incompressible couple stress fluid between two parallel plates that are situated at $y = -l$ and $y = l$. In this case, there is no pressure gradient $(G = 0)$ for the fluid flow between the plates. The flow is caused by plates motion. The lower and upper plates are thought to be moving at constant translational rates u_2 and u_1, respectively. The boundary conditions for the plane Couette flow are

$$u(-1) - \delta \left(\frac{du}{dy} - s^2 \frac{d^3u}{dy^3} \right) \bigg|_{y=-1} = \sigma, \quad u(1) + \delta \left(\frac{du}{dy} - s^2 \frac{d^3u}{dy^3} \right) \bigg|_{y=1} = 1, \tag{11}$$

$$\frac{d^2u}{dy^2}\bigg|_{y=-1} = \xi \frac{du}{dy}\bigg|_{y=-1}, \quad \frac{d^2u}{dy^2}\bigg|_{y=1} = -\xi \frac{du}{dy}\bigg|_{y=1}, \tag{12}$$

where $\delta = \alpha/l$ and $\xi = \gamma/\left(4\,\mu\, s^2\right)$ are the non-dimensional velocity slip and couple stress spin slip parameters, respectively, and σ is the velocity ratio between the lower and upper plates, i.e., $\sigma = u_2/u_1$. The solution of (7) is

$$u^{CF} = A_1 + B_1 y + C_1 e^{y/s} + D_1 e^{-y/s}, \tag{13}$$

where

$$A_1 = \frac{1}{2}\left(\sigma + 1\right), \qquad B_1 = -\frac{1}{\Delta}\left[\sigma(G_1 e^{2/s} + G_2) - G_1 e^{2/s} - G_2\right],$$
$$C_1 = \frac{1}{\Delta}\left[s^2 \xi e^{1/s}(\sigma - 1)\right], \qquad D_1 = -\frac{1}{\Delta}\left[s^2 \xi e^{1/s}(\sigma - 1)\right].$$

After substituting the values of A_1, B_1, C_1, D_1 in (13), we get the velocity u^{CF}, the volume flow rate Q^{CF}, the vorticity ω_z^{CF}, and the couple stress m_{yz}^{CF} for the plane Couette flow as follows

$$u^{CF} = \frac{y\, G_5 + e^{y/s} G_4 - e^{-y/s} G_4}{\Delta} + \frac{\sigma + 1}{2}, \tag{14}$$

$$Q^{CF} = \sigma + 1, \tag{15}$$

$$\omega_z^{CF} = -\frac{1}{2}\left(\frac{s\, G_5 + G_4\, e^{y/s} + G_4\, e^{-y/s}}{\Delta s} \right), \tag{16}$$

$$m_{yz}^{CF} = -2\,\eta\, G_4 \left(\frac{e^{y/s} - e^{-y/s}}{\Delta s^2} \right), \tag{17}$$

where

$$\Delta = 2\left(\delta G_3 + G_8 e^{2/s} + s\,\xi\, G_7 - 1\right), \quad G_1 = s\,\xi + 1, \quad G_2 = s\,\xi - 1,$$
$$G_3 = G_1 e^{2/s} + G_2, \quad G_4 = s^2\,\xi(\sigma - 1)e^{1/s}, \quad G_5 = G_2 - \sigma G_3 + e^{2/s} G_1,$$
$$G_6 = 1 - s, \quad G_7 = 1 + s, \quad G_8 = s\,\xi\, G_6 + 1.$$

2.3. Plane Poiseuille flow (PF)

This flow is carried by a constant pressure gradient G in positive x-direction with the assumptions of both plates are at rest ($u_1 = 0$, $u_2 = 0$). The boundary conditions for the plane Poiseuille flow are

$$u(-1) - \delta\left(\frac{du}{dy} - s^2\frac{d^3u}{dy^3}\right)\bigg|_{y=-1} = 0, \qquad u(1) + \delta\left(\frac{du}{dy} - s^2\frac{d^3u}{dy^3}\right)\bigg|_{y=1} = 0, \tag{18}$$

along with the spin slip boundary conditions (12) and (18), the solution of (7) is

$$u^{PF} = A_2 + B_2 y + C_2\cosh(cy) + D_2\sinh(cy) - \frac{Gy^2}{2}, \tag{19}$$

where

$$A_2 = \frac{2G\delta H_1 + G(H_1 - 2H_2)}{2H_1}, \quad B_2 = 0, \quad C_2 = \frac{GH_2}{H_1}, \quad D_2 = 0.$$

After substituting the values of A_2, B_2, C_2, D_2 in (19), we get the velocity u^{PF}, the volume flow rate Q^{PF}, the vorticity ω_z^{PF}, and the couple stress m_{yz}^{PF} for the plane Poiseuille flow as

$$u^{PF} = \frac{2\,GH_2\cosh(cy) + GH_1H_3 - 2\,GH_2\cosh(c)}{2\,H_1} - \frac{Gy^2}{2}, \tag{20}$$

$$Q^{PF} = \frac{(6GH_2(\sinh(c) - c\cosh(c)) + (3\,GH_1H_3 - H_1)c}{3\,c\,H_1}, \tag{21}$$

$$\omega_z^{PF} = -\frac{1}{2}\left(\frac{GH_2c\sinh(cy)}{H_1} - Gy\right), \tag{22}$$

$$m_{yz}^{PF} = -2\,\eta\left(\frac{GH_2c^2\cosh(cy)}{H_1} - G\right), \tag{23}$$

where

$$H_1 = \xi c\sinh(c) + c^2\cosh(c), \quad H_2 = \xi + 1, \quad H_3 = 1 + 2\,\delta, \quad c = \frac{1}{s}.$$

2.4. Generalized Couette flow (GCF)

In this flow problem, the lower plate is assumed to be at rest $(u_2 = 0)$, while the upper plate is moving at a constant speed u_1. The pressure gradient G is constant. The boundary conditions for the generalized Couette flow are

$$u\,(-1) - \;\delta\left(\frac{du}{dy} - s^2\frac{d^3u}{dy^3}\right)\bigg|_{y=-1} = 0, \qquad u\,(1) + \;\delta\left(\frac{du}{dy} - s^2\frac{d^3u}{dy^3}\right)\bigg|_{y=1} = 1, \tag{24}$$

along with the spin slip boundary conditions (12) and (24), the solution of (7) is

$$u^{GCF} = A_3 + B_3 y + C_3\cosh(cy) + D_3\sinh(cy) - \frac{Gy^2}{2}, \tag{25}$$

where

$$A_3 = \frac{(2G\delta + 1)H_1 + G(\xi c\sinh(c) + c^2 - 2H_2)}{2H_1}, \qquad B_3 = \frac{F_1}{2(\delta F_1 + F_1 - \xi\sinh(c))},$$

$$C_3 = \frac{GH_2}{H_1}, \qquad D_3 = -\frac{\xi}{2(\delta F_1 + F_1 - \xi\sinh(c))}.$$

After substituting the values of A_3, B_3, C_3, D_3 in (25), the velocity u^{GCF}, the volume flow rate Q^{GCF}, the vorticity ω_z^{GCF} and the couple stress m_{yz}^{GCF} for the generalized Couette flow are

$$u^{GCF} = \frac{yF_1 - \xi \sinh(cy)}{F_3} + \frac{2G\cosh(cy)\,H_2 + 2G\,F_5 + F_4F_2}{2F_2} - \frac{Gy^2}{2}, \tag{26}$$

$$Q^{GCF} = \frac{6H_2G\sinh(c) + [(6F_5 - F_2)\,G + 3F_2F_4]}{3cF_2}, \tag{27}$$

$$\omega_z^{GCF} = -\frac{1}{2}\left(\frac{F_1 - \xi c\cosh(cy)}{F_3} + \frac{GH_2c\sinh(cy)}{F_2} - Gy\right), \tag{28}$$

$$m_{yz}^{GCF} = -2\,\eta\left(\frac{GH_2c^2\cosh(cy)}{F_2} - \frac{\xi c^2\sinh(cy)}{F_3} - G\right), \tag{29}$$

where

$$F_1 = \xi c\cosh(c) + c^2\sinh(c), \qquad F_2 = \xi c\sinh(c) + c^2\cosh(c),$$
$$F_3 = 2F_1(\delta+1) - 2\xi\sinh(c), \qquad F_4 = 1 + G, \qquad F_5 = \delta F_2 - H_2\cosh(c).$$

3. Results and discussion

In this analysis, we have derived the analytical solutions for couple stress fluid flow between parallel plates, utilizing spin slip conditions at the upper and lower plates. Tables 1–3 present the velocity profile, skin friction and volume flow rate for the various cases involving the spin slip parameters. The quantities used in these tables are defined as follows:

$$\begin{aligned}
&X_1 = e^{2/s} + 1, && Y_1 = c\sinh(c), && Z_5 = 2Gc\cosh(c),\\
&X_2 = s + 1 + (1-s)\,e^{2/s}, && Z_1 = c\cosh(c) - \sinh(c), && Z_6 = (3G+1)\,c^2Z_3,\\
&X_3 = e^{2/s} - 1, && Z_2 = \delta c\cosh(c) + Z_1, && Z_7 = 2GZ_3c^2\delta^2,\\
&X_4 = 1 - \sigma, && Z_3 = \cosh(c)\sinh(c), && Z_8 = (G+1)\,Z_4Z_1 - 2GZ_1\cosh(c),\\
&X_5 = \sigma + 1, && Z_4 = c\sinh(c), && Z_9 = Z_5\,(\cosh(cy) - \cosh(c)).
\end{aligned}$$

The variations of the following different parameters on the velocity profile, volume flow rate, vorticity, and couple stresses for each problem are analyzed:

1. couple stress spin slip parameter $(0 < \xi < \infty)$ [10, 11],
2. pressure gradient $(0 \le G < \infty)$ [10],
3. velocity slip parameter $(0 < \delta < \infty)$ [10, 11, 20],
4. couple stress parameter $(0 \le s < \infty)$ [10, 16, 20].

A demonstration of the influence of the spin slip parameter ξ on velocity profiles for the Couette, Poiseuille, and generalized Couette flows can be seen in Fig. 2. In Fig. 2a, we have noticed that as the spin slip parameter increases for the plane Couette flow $(\sigma = 0)$, the fluid velocity rises near the lower plate, whereas the trend reverses near the upper plate. Fig. 2b depicts the velocity profile for the Poiseuille flow $(\sigma = 1)$, which is parabolic and symmetric. This graph indicates the fluid velocity is at its maximum at the center between the plates and decreases progressively toward the plates, where fluid particles are in contact with the plates having zero velocity. In Fig. 2c, we examine the variation of fluid velocity for the generalized Couette flow $(\sigma = -1)$. Here, we see that as the spin slip parameter increases, velocity of the fluid grows, and reaches its maximum at the center between the plates. The fluid velocity is zero at the stationary plate (bottom) because the lower plate does not slip at the surface of the fluid particles. Conversely,

Table 1. Velocity profiles for (I) plane Couette flow (CF), (II) plane Poiseuille flow (PF), (III) generalized Couette flow (GCF)

	Velocity profile for a non-zero couple stress slip parameter ξ (new result)	Velocity profile for $\xi = 0$, i.e., zero couple stress spin slip parameter [10]	Velocity profile when $\xi \to \infty$, i.e., zero vorticity (new result)
I	$\frac{yG_5+e^{y/s}G_4- e^{-y/s}G_4}{\Delta} + \frac{\sigma+1}{2}$	$\frac{1}{2}\left(1+\frac{y}{\delta+1}\right)+\frac{\sigma}{2}\left(1-\frac{y}{\delta+1}\right)$	$\frac{X_1X_5e^{y/s}\delta-X_4se^{(2y+1)/s}}{2X_1e^{y/s}(s+1)-2X_3se^{y/s}} + \frac{(X_1X_4+X_2X_5)e^{y/s}-X_5se^{y/s}}{2X_1e^{y/s}(s+1)-2X_3se^{y/s}}$
II	$\frac{2GH_2\cosh(cy)+GH_1H_3}{2H_1}$ $\frac{-2GH_2\cosh(c)}{2H_1} - \frac{Gy^2}{2}$	$\frac{G}{2}\left(1+2\delta-y^2\right) - \frac{G}{c^2}\left(1-\frac{\cosh(cy)}{\cosh(c)}\right)$	$\frac{2G(Y_1\delta+\cosh(cy))+GY_1}{Y_1} - \frac{GY_1y^2-2G\cosh(c)}{Y_1}$
III	$\frac{yF_1-\xi\sinh(cy)}{F_3} - \frac{Gy^2}{2} + \frac{2GH_2\cosh(cy)+2GF_5+F_4F_2}{2F_2}$	$\frac{G}{2}\left(1-y^2\right) + \frac{1}{2}\left(1+2\delta G-\frac{y}{\alpha+1}\right) - \frac{G}{c^2}\left(1-\frac{\cosh(cy)}{\cosh(c)}\right)$	$\frac{Z_7-Z_4\sinh(cy)+2GZ_1\cosh(cy)}{2Z_4Z_2} + \frac{\left[Z_9\,\delta-GZ_4(cy^2\cosh(c)+2\sinh(c))\right]\delta}{2\,Z_2\,Z_4} + \frac{Z_6\delta+c^2Z_3y-GZ_4Z_1y^2+Z_8}{2Z_4Z_2}$

Table 2. Non-dimensional skin friction for (I) CF, (II) PF, (III) GCF

	Non-dimensional skin friction ($t^*_{yx} = lt_{yx}/\mu u_1$) for non-zero couple stress spin slip parameter ξ	Skin friction t^*_{yx} when $\xi = 0$, i.e., zero couple stress spin slip parameter	Skin friction t^*_{yx} when $\xi \to \infty$, i.e., zero vorticity
I	$\frac{e^2G_1(\sigma-1)+G_2(\sigma-1)}{2e^{2/s}[G_1(\delta+1)-s^2\xi]+2[G_2(\delta+1)+s^2\xi]}$	$\frac{\sigma-1}{2\delta+2}$	$\frac{X_1X_5e^{y/s}\delta-X_4se^{(2y+1)/s}}{2X_1e^{y/s}(s+1)-2X_3se^{y/s}}$
II	Gy	Gy	Gy
III	$Gy - \frac{\xi c\cosh(c)+c^2\sinh(c)}{2\xi c(\delta+1)\cosh(c)+2[c^2(\delta+1)-\xi]\sinh(c)}$	$\frac{2Gy(\delta+1)-1}{2(\delta+1)}$	$\frac{c[2Gy(\delta+1)-1]\cosh(c)-2G\sinh(c)}{2(\delta+1)\cosh(c)}$

Table 3. Volume flow rate for (I) CF, (II) PF, (III) GCF

	Volume flow rate for non-zero couple stress spin slip parameter ξ	Volume flow rate when $\xi = 0$, i.e., zero couple stress spin slip parameter	Volume flow rate for $\xi \to \infty$, i.e., zero vorticity
I	$\sigma+1$	$\sigma+1$	$\sigma+1$
II	$\frac{6GH_2(\sinh(c)-c\cosh(c))}{3cH_1} + \frac{c(3GH_1H_3-H_1)}{3cH_1}$	$\frac{6G(\sinh(c)-c\cosh(c))}{3c^3\cosh(c)} + \frac{(3GH_3-1)}{3}$	$\frac{6G(\sinh(c)-c\cosh(c))}{3c^2\sinh(c)} + \frac{(3GH_3-1)}{3}$
III	$\frac{6GH_2\sinh(c)}{3cF_2} + \frac{[3F_2F_4+G(6F_5-F_2)]}{3cF_2}$	$\frac{6G\sinh(c)+3F_2c^2\cosh(c)}{3c^3\cosh(c)} + \frac{G(6\delta c^2-6-c^2)}{3c^3}$	$\frac{6G\sinh(c)+3cF_4\sinh(c)}{3c^2\sinh(c)} + \frac{G[c\sinh(c)(6\delta-1)-6\cosh(c)]}{3c^2\sinh(c)}$

the fluid velocity is non-zero near the upper plate, so the upper plate slips at fluid surface leading to an increase in velocity near the upper plate. Additionally, we note that the spin effect of particles on the surface of stationary plates is negligible, while this effect is maximized in the middle between the plates. In fluid flows, particles can partially rotate independently of the boundary, as controlled by the spin slip parameter.

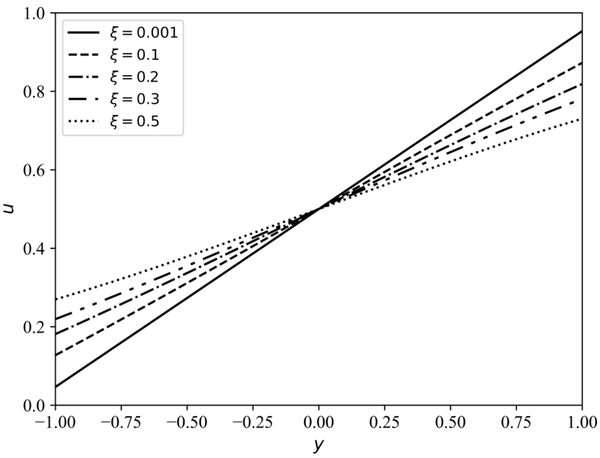

(a) CF when $s = 0.5,\ \delta = 0.1$

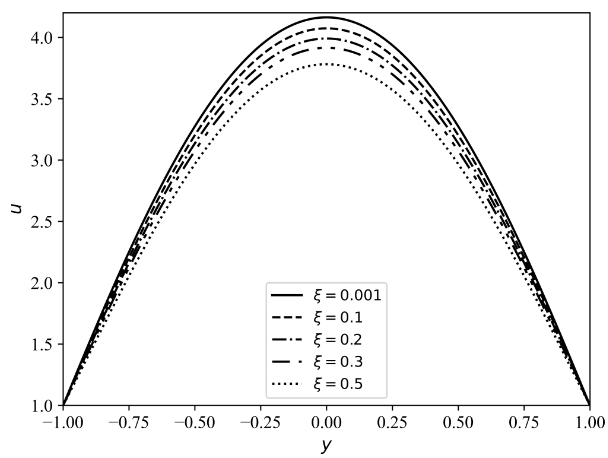

(b) PF when $s = 0.5,\ \delta = 0.1,\ G = 10$

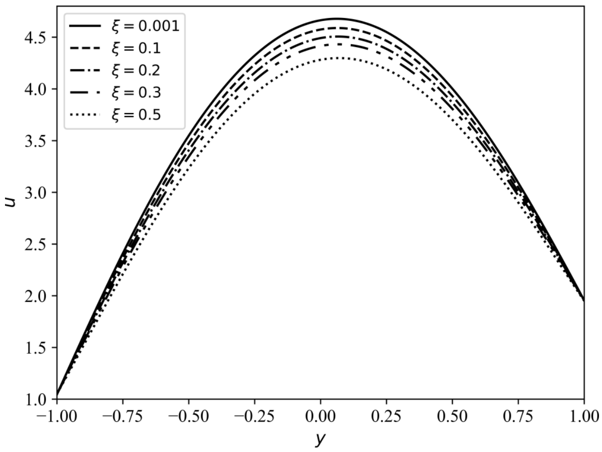

(c) GCF when $s = 0.5,\ \delta = 0.1,\ G = 10$

Fig. 2. Analysis of velocity profile for the spin slip parameter ξ

For the Poiseuille and generalized Couette flows, Fig. 3 illustrates the relation between the volume flow rate and the pressure gradient G for various values of the spin slip parameter. In Fig. 3a, we observe that the volume flow rate increases as the pressure gradient grows. This phenomenon occurs because an increase in the pressure gradient indicates a greater force exerted on the fluid particle per unit area (wall shear stress), which subsequently enhances the fluid flow of the particles. Hence, the volume flow rate increases. Similarly, Fig. 3b shows that as the pressure gradient grows, the volume flow rate also grows. The identical reason for this behavior is consistent with our observation in Fig. 3a. Additionally, it is noteworthy that the volume flow rate exhibits more variation at lower values of the spin slip parameter. The reason behind is the fact that the spin slip contributes to the energy dissipation in fluid by allowing rotational energy to be lost through slippage.

Fig. 4 illustrates the effect of the spin slip parameter on the volume flow rate Q with the velocity slip parameter. In Fig. 4a, it is shown that as the velocity slip parameter increases, the volume flow rate also rises. A non-zero velocity slip parameter indicates reduced resistance between the fluid particles and the plates, so the volume flow rate increases when the velocity slip parameter grows. The same trend is observed in Fig. 4b, as seen in Fig. 4a for the generalized Couette flow. It has been found that at low values of the spin slip parameter, the volume flow rate is significantly higher.

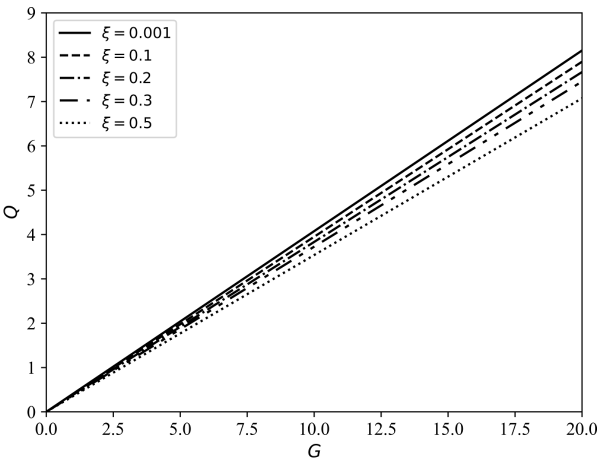

(a) PF

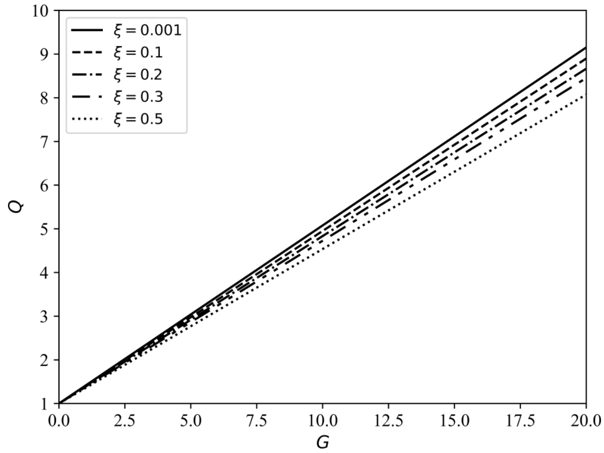

(b) CGF

Fig. 3. Analysis of volume flow rate for ξ when $s = 0.5,\ \delta = 0$

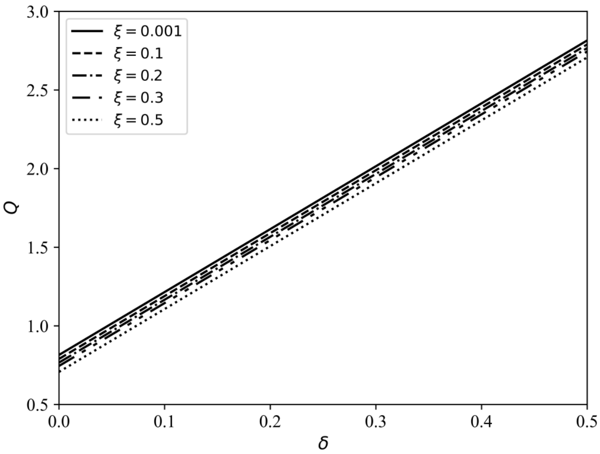

(a) PF

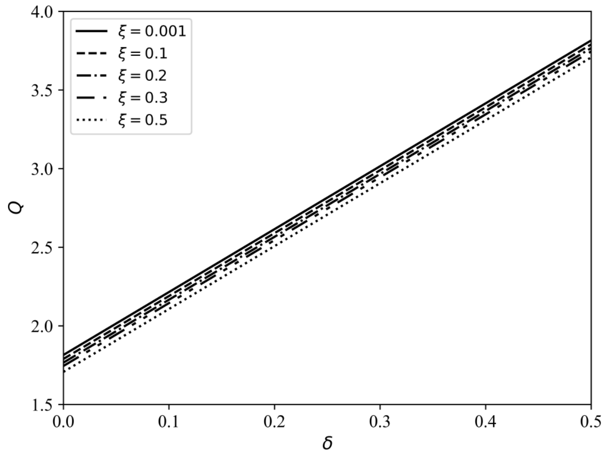

(b) CGF

Fig. 4. Analysis of volume flow rate for ξ when $s = 0.5, G = 2$

Fig. 5 reveals the description of the link between the volume flow rate, the couple stress parameter, and the spin slip parameter. From Fig. 5a, it is evident that the volume flow rate decreases with increasing couple stress parameter. This decrease occurs because the viscosity (or thickness) of a couple stress fluid shows higher values compared to the Newtonian fluid. It is more evident in the generalized Couette flow compared to the Poiseuille flow, as shown in Fig. 5b. Also, it is observed that the volume flow rate is a decreasing function of the spin slip parameter.

The vorticity vector describes the rotation of fluid particles. In couple stress fluids, this rotation is significant because it contributes directly to the shear stress due to couple stresses. As shown in Fig. 6, the variation of the non-dimensional vorticity for a variety of spin slip parameters is presented. Fig. 6a demonstrates that the vorticity is the highest at the center between the plates and displays the greatest variation for the highest value of the spin slip parameter. Fig. 6b shows that for larger values of the spin slip parameter, the changes of fluid vorticity are more prominent, with vorticity decreasing from the lower plate to the upper plate. In Fig. 6c, we observe similar curve patterns as in Fig. 6b. Notably, the variation of vorticity for the generalized Couette flow is greater than that of the Poiseuille flow due to the motion of the upper plate.

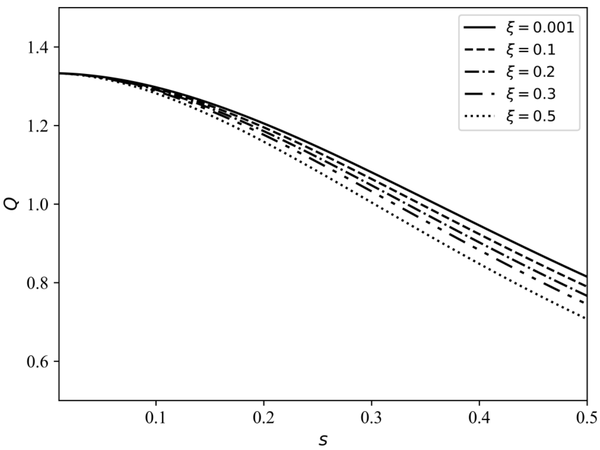

(a) PF

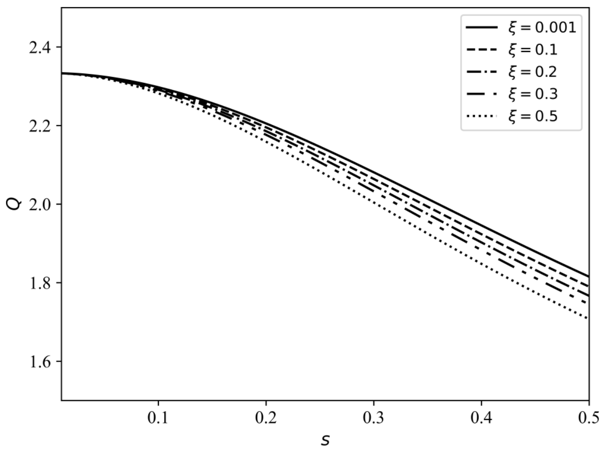

(b) CGF

Fig. 5. Analysis of volume flow rate for ξ when $\delta = 0, G = 2$

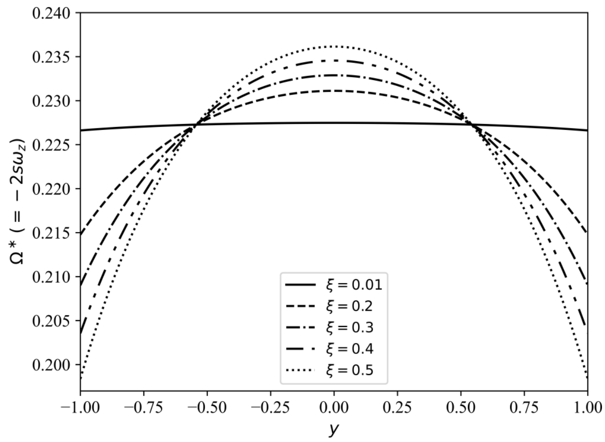

(a) CF when $s = 0.5,\ \delta = 0.1$

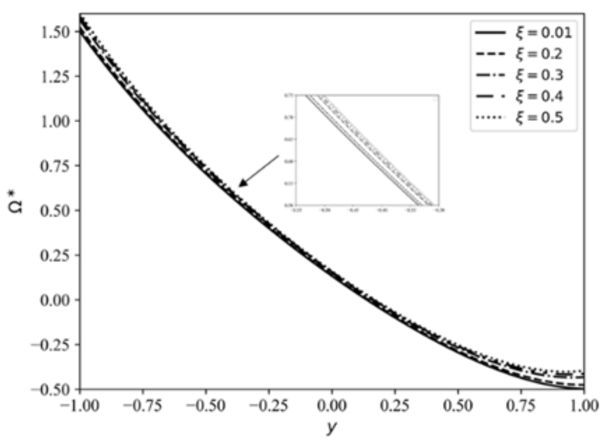

(b) PF when $s = 0.5,\ \delta = 0.1,\ G = 2$

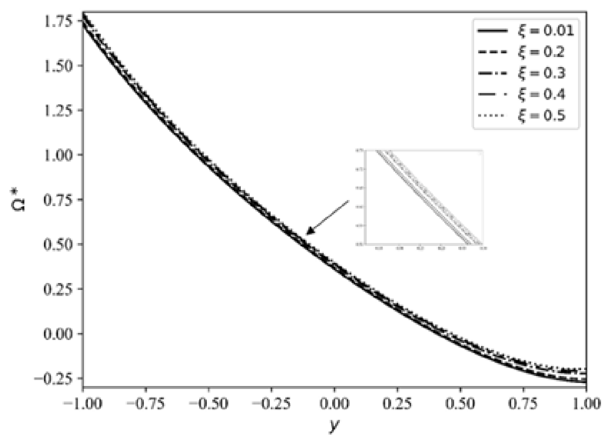

(c) GCF when $s = 0.5,\ \delta = 0.1,\ G = 2$

Fig. 6. Analysis of non-dimensional vorticity for ξ

The formulas (17), (23), and (29) for the couple stress refer to a specific type of stress in the fluid that takes impact of moment or torque with shear and normal stresses. Fig. 7 illustrates the variation of the non-dimensional couple stress for different values of the spin slip parameter. In Fig. 7a, it is observed that as the spin slip parameter increases, the couple stress on the lower

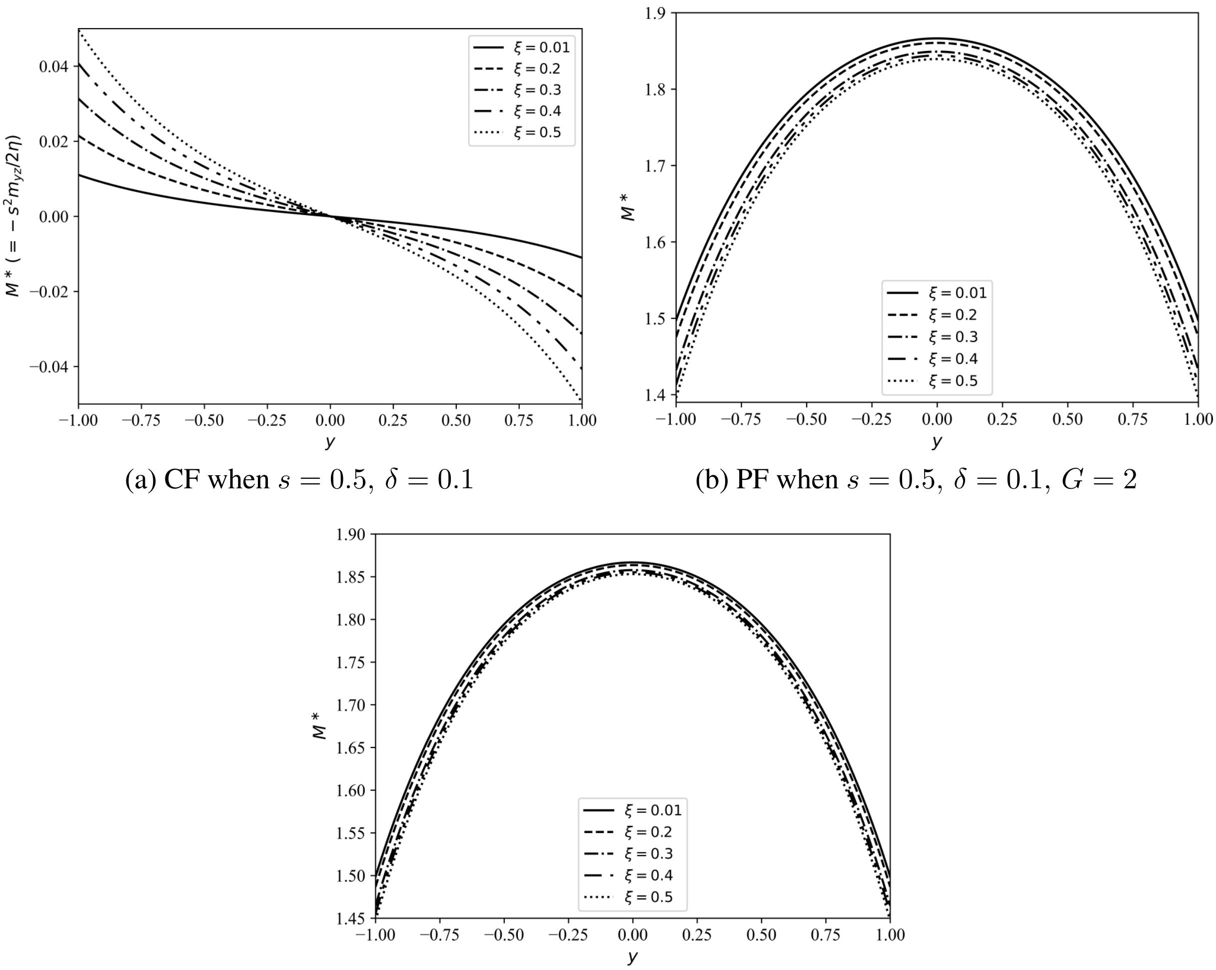

(a) CF when $s = 0.5,\ \delta = 0.1$

(b) PF when $s = 0.5,\ \delta = 0.1,\ G = 2$

(c) GCF when $s = 0.5,\ \delta = 0.1,\ G = 2$

Fig. 7. Analysis of non-dimensional couple stress for ξ

plate also increases, while the opposite effect occurs on the upper plate. The couple stress represents a form of stress that arises not only from shear stress but also from local rotations of fluid particles. These rotational stresses are captured by the couple stress tensor, which describes the fluid's resistance to rotational deformations. In Fig. 7b, we see that the couple stress increases with decreasing values of the spin slip parameter, showing maximum couple stress at the center between the plates. A similar pattern of curves can be noted in the case of the generalized Couette flow, as represented in Fig. 7c. For further details on the impact of the tangential slip on the velocity and the volume flow rate, one can refer to the work by Devakar et al. [10].

4. Conclusions

The primary goal of this paper is to explore the effect of couple stress and spin slip on the couple stress fluid flow between two parallel plates. The boundary conditions at the solid surface include non-vanishing tangential and couple stress spin slip conditions. The expressions for the velocity profile, volume flow rate, vorticity and couple stress are obtained. The impact of various parameters, such as the couple stress spin slip parameter, velocity slip parameter, pressure gradient, and couple stress parameter, on the velocity profile, volume flow rate, vorticity, and couple stress is analyzed from the presented figures and tables. We draw the following key conclusions:

1. It is found that the fluid velocity, couple stress, and volume flow rate decrease with an increase in the spin slip parameter.
2. The volume flow rate grows with the higher pressure gradient and the velocity slip parameter, while it diminishes as the couple stress parameter increases.
3. The vorticity of the fluid particles increases alongside the spin slip parameter.
4. We have observed that the spin slip parameter has no impact on the volume flow rate for the Couette flow.

Notably, the limiting solutions as $\xi \to 0$ are in agreement with those published by Devakar et al. [10], which addressed the case of vanishing couple stress at the boundary. The present work has various applications in industrial and biological processes because the spin slip conditions provide a more accurate representation of micro-scale flow properties and wall boundary responses, making them essential for predicting flow characteristics and stress distributions. For future research, non-Newtonian fluid flow with various geometries under spin slip effect can be considered.

Acknowledgements

The first author, Shekhar Nishad, expresses gratitude for the fellowship from the National Institute of Technology Raipur. The authors are thankful to Prof. M. Devakar, Visvesvaraya National Institute of Technology Nagpur, India for his valuable suggestions which led to the improvement of the manuscript.

References

[1] Ahmad, A., Ishaq, A., Athar, M., Anjum, J., Nawaz, R., Unsteady flow of micropolar fluid on a magnetized sheet: Effects of magnetic and microrotation parameters on wall couple stress and skin friction, ZAMM – Journal of Applied Mathematics and Mechanics / Zeitschrift für Angewandte Mathematik und Mechanik 103 (11) (2023) No. e202100571. https://doi.org/10.1002/zamm.202100571

[2] Akhtar, S., Shah, N. A., Exact solutions for some unsteady flows of a couple stress fluid between parallel plates, Ain Shams Engineering Journal 9 (4) (2018) 985–992. https://doi.org/10.1016/j.asej.2016.05.008

[3] Alamri, S. Z., Ellahi, R., Shehzad, N., Zeeshan, A., Convective radiative plane Poiseuille flow of nanofluid through porous medium with slip: An application of Stefan blowing, Journal of Molecular Liquids 273 (2019) 292–304. https://doi.org/10.1016/j.molliq.2018.10.038

[4] Alotaibi, M. A., El-Sapa, S., MHD couple stress fluid between two concentric spheres with slip regime, Results in Engineering 21 (2024) No. 101934. https://doi.org/10.1016/j.rineng.2024.101934

[5] Ashmawy, E., Unsteady Couette flow of a micropolar fluid with slip, Meccanica 47 (2012) 85–94. https://doi.org/10.1007/s11012-010-9416-7

[6] Asia, Y., Kashif, A., Muhammad, A., MHD unsteady flow and heat transfer of micropolar fluid through porous channel with expanding or contracting walls, Journal of Applied Fluid Mechanics 9 (4) (2016) 1 807–1 817. https://doi.org/10.18869/acadpub.jafm.68.235.22857

[7] Chamkha, A. J., El-Kabeir, S., Rashad, A., Unsteady coupled heat and mass transfer by mixed convection flow of a micropolar fluid near the stagnation point on a vertical surface in the presence of radiation and chemical reaction, Progress in Computational Fluid Dynamics, An International Journal 15 (3) (2015) 186–196. https://doi.org/10.1504/PCFD.2015.069576

[8] Chen, Y.-L., Zhu, K.-Q., Couette–Poiseuille flow of Bingham fluids between two porous parallel plates with slip conditions, Journal of Non-Newtonian Fluid Mechanics 153 (1) (2008) 1–11. https://doi.org/10.1016/j.jnnfm.2007.11.004

[9] Devakar, M., Iyengar, T., Run up flow of a couple stress fluid between parallel plates, Nonlinear Analysis: Modelling and Control 15 (1) (2010) 29–37. https://doi.org/10.15388/NA.2010.15.1.14362

[10] Devakar, M., Sreenivasu, D., Shankar, B., Analytical solutions of couple stress fluid flows with slip boundary conditions, Alexandria Engineering Journal 53 (3) (2014) 723–730. https://doi.org/10.1016/j.aej.2014.06.005

[11] El-Sapa, S., Almoneef, A. A., The axisymmetric migration of an aerosol particle embedded in a Brinkmann medium of a couple stress fluid with slip regime, European Journal of Pure and Applied Mathematics 15 (4) 1 566–1 592. https://doi.org/10.29020/nybg.ejpam.v15i4.4549

[12] Ellahi, R., Effects of the slip boundary condition on non-Newtonian flows in a channel, Communications in Nonlinear Science and Numerical Simulation 14 (4) (2009) 1 377–1 384. https://doi.org/10.1016/j.cnsns.2008.04.002

[13] Hayat, T., Khan, M., Ayub, M., Couette and Poiseuille flows of an Oldroyd 6-constant fluid with magnetic field, Journal of Mathematical Analysis and Applications 298 (1) (2004) 225–244. https://doi.org/10.1016/j.jmaa.2004.05.011

[14] Kamran, M. M., Siddique, I., MHD Couette and Poiseuille flow of a third grade fluid, Open Journal of Mathematical Analysis 1 (2) (2017) 1–19. https://doi.org/10.30538/psrp-oma2017.0006

[15] Khalid, A., Khan, I., Khan, A., Shafie, S., Conjugate transfer of heat and mass in unsteady flow of a micropolar fluid with wall couple stress, AIP Advances 5 (12) (2015) No. 127125. https://doi.org/10.1063/1.4938551

[16] Madasu, K. P., Sarkar, P., Couple stress fluid past a sphere embedded in a porous medium, Archive of Mechanical Engineering 69 (1) (2022) 5–19. https://doi.org/10.24425/ame.2021.139314

[17] Navier, C. L. M. H., Memoir on the laws of fluid motion, Mmoires de lAcadmie des sciences, 1822. (in French)

[18] Neto, C., Evans, D. R., Bonaccurso, E., Butt, H.-J., Craig, V. S., Boundary slip in Newtonian liquids: A review of experimental studies, Reports on Progress in Physics 68 (12) (2005) No. 2859. https://doi.org/10.1088/0034-4885/68/12/R05

[19] Ramesh, K., Effects of viscous dissipation and Joule heating on the Couette and Poiseuille flows of a Jeffrey fluid with slip boundary conditions, Propulsion and Power Research 7 (4) (2018) 329–341. https://doi.org/10.1016/j.jppr.2018.11.008

[20] Sarkar P., Madasu, K. P., Impact of couple stresses on slow rotation of a slip sphere: Brinkman's medium, International Journal of Applied and Computational Mathematics 10 (2024) No. 116. https://doi.org/10.1007/s40819-024-01749-x

[21] Stokes, V. K., Theories of fluids with microstructure: An introduction, Springer Science & Business Media, 2012. https://doi.org/10.1007/978-3-642-82351-0

[22] Zeeshan, A., Shehzad, N., Ellahi, R., Alamri, S. Z., Convective Poiseuille flow of Al_2O_3–EG nanofluid in a porous wavy channel with thermal radiation, Neural Computing and Applications 30 (11) (2018) 3 371–3 382. https://doi.org/10.1007/s00521-017-2924-9